ARTICLE

Insights into Elastic and Thermodynamics Properties of Binary Intermetallics in Ni-Al Alloys under Extreme Condition: Full-Electronic Quasi-Harmonic Study

Yong-song Luo, Yu-ping Cang, Dong Chen*

College of Physics and Electronic Engineering, Xinyang Normal University, Xinyang 464000

(Dated: Received on April 27, 2014; Accepted on June 16, 2014)

Atomistic modeling based on the accurate first-principles method is used to investigate the lattice parameter, elastic constant, elastic modulus including bulk modulus (B) and shear modulus (G), Poisson's ratio, and elastic anisotropy of Al, NiAl and Ni_3Al under extreme condition. The elastic constants obtained from calculations meet their mechanical stability criteria. Both NiAl and Ni_3Al exhibit ductile behavior due to their high bulk mudulus to shear modulus ratios of B/G ratios. Through the full-electronic quasi-harmonic approximation, in which the mobile electrons are considered, we successfully obtain the thermo-physical properties including the thermal expansion coefficient, bulk modulus, heat capacity and entropy at simultaneously high temperatures and high pressures. The calculated quantities agree well with the available results. Some silent results are also interpreted. Several interesting features in the thermodynamic properties can also be observed.

Key words: First-principles, Heat capacity, Bulk modulus, Debye approximation

I. INTRODUCTION

Due to the valuable properties such as light weight, high elastic moduli, good corrosion resistance, excellent thermal conductivity, and large plasticity [1], Al, NiAl, and Ni_3Al are especially amenable to be used in space project. As a metallic element without d-electrons, a relatively low atomic mass and a simple structure, Al can be used as a reference material in modern industry. It has been known for several decades that aluminum has a face-centered cubic structure at room temperature (space group: *Fm-3m*). Al can retain its mechanical stability up to 220 GPa [2]. Upon further compression, it will transform into a new phase, which has a hexagonal close-packed structure (hcp-Al) [2, 3]. The Ni-Al binary alloys have been used as high-temperature materials for gas turbines and aircraft engines. These alloys also belong to the engineering materials with attractive properties including good high-temperature strength, resistance to oxidation and low density [4, 5]. The Ni-Al alloys for structural applications in energy conversion systems are currently under development [6−9]. NiAl and Ni_3Al crystallize in cubic structures (space group: *Pm-3m*). The Ni and Al atoms (NiAl) occupy the (0.5, 0.5, 0.5) and (0, 0, 0) Wyckoff positions [4], respectively. Different atoms in Ni_3Al occupy the Al (0, 0, 0) and Ni (0.5, 0, 0.5) sites [10].

*Author to whom correspondence should be addressed. E-mail: chchendong2010@163.com, FAX: +86-376-6391731

First-principles technique including lattice dynamics and phonon approaches has been widely used and are now indispensable for condensed-matter physics. One shortcoming is that the pressure and temperature effects can not be simultaneously considered. Blanco *et al.* have developed a "quasi-harmonic Debye" approach (QHD) [11], in which some fundamental thermal properties of solids can be obtained at high temperature and high pressure. Unfortunately, the QHD scheme is not suitable for metals since the mobile electron contributions to the Gibbs free energy are not taken into account in this scheme. As an all-known fact, there are many free electrons in metals and alloys. These highly mobile electrons can not be ignored, especially at high temperatures.

The temperature and pressure dependences of thermodynamic quantities can directly provide useful information for understanding the dynamical response of solids [12]. Although the elastic and thermodynamic properties of Al, NiAl and Ni_3Al have been widely investigated from experiment [6, 8, 13−15] to theory [7, 16−23], the pressure P was often restricted to 0 GPa and the mobile electron contributions were usually ignored. Take Ni as an example, the electronic contribution to the heat capacity was 28% of heat capacity at 1000 K [19].

In this work, we investigate the thermodynamic properties of Ni_xAl (x=0, 1 and 3) at simultaneously high temperature and high pressure by the recently developed full-electronic quasi-harmonic approximation (FE-QHA) sheme to obtain the high-temperature and high-pressure properties of solids, the mobile electrons are

DOI:10.1063/1674-0068/27/04/399-406

considered at high pressures and high temperatures.

II. METHOD OF CALCULATION

We firstly do the total energy calculations by performing the first-principles plane-wave pseudo-potential (PW-PP) method [24]. The exchange-correlation functional is treated by the generalized gradient approximation (GGA) of the PBE form [25]. Reference configurations for the valence electrons are Ni3d^{8}4s^2 and Al3s^{2}3p^1. According to the convergence tests, the cutoff energies are chosen to be 500 eV. The Monkhorst-Pack k-points [26] are 14×14×14, 15×15×15, and 15×15×15 for Al, NiAl, and Ni_3Al, respectively. The convergence of the total energy is 0.2 μeV/atom. The phonon density of state is calculated through the finite displacement method combined with the norm-conserving pseudo-potentials [27]. For the super-cell (48 unit cells), we use a cutoff radius of 5.0 Å in order to obtain the accurate results. The q-vector is chosen to be 9×9×9. For such simple structures, these parameters are suitable for the phonon calculations.

The k-points are determined by the equation $(1/a{:}1/b{:}1/c)$, where a, b, and c are the lattice constants. For the cubic Al, NiAl, and Ni_3Al, the $1/a{:}1/b{:}1/c$=1:1:1. The k-point mesh should be 3×3×3, or 4×4×4, or 11×11×11, *etc.* According to our convergence tests, the plane-wave cutoff 500 eV and the k-points 14×14×14 can generate good results for Al. The adequate parameters for NiAl and Ni_3Al are found to be 500 eV (cutoff energy) and 15×15×15 (k-points).

The main advantage of the calculation of pressure and temperature dependent properties of solids is the easiness with which extreme conditions, unattainable by experimental means, can be modeled and determined. Then FEQHA sheme is implemented to obtain the high-temperature and high-pressure properties of solids. This method has been described in detail elsewhere (see Refs. [28, 29]), here we give a brief overview for completeness. In the FEQHA scheme, the non-equilibrium Gibbs free energy $G^*(V;P,T)$ can be determined by

$$G^*(V;P,T) = E(V) + PV + F_{\rm vib}(V;T) + F_{\rm el}(V;T) \quad (1)$$

where $E(V)$ is the total energy. PV represents the hydrostatic pressure condition. $F_{\rm vib}$ and $F_{\rm el}$ are the contributions to the Helmholtz free energy from atomic vibrations and mobile electrons, respectively.

$$F_{\rm vib}(V;T) = \sum_{j=1}^{3nN}\left[\frac{\omega_j}{2} + k_{\rm B}T\ln(1-{\rm e}^{-\omega_j/k_{\rm B}T})\right] \quad (2)$$

$$F_{\rm el}(V;T) = E_{\rm el} - TS_{\rm el} \quad (3)$$

$$E_{\rm el}(V;T) = \int n(\varepsilon,V)f(\varepsilon){\rm d}\varepsilon - \int^{\varepsilon_F} n(\varepsilon,V)\varepsilon{\rm d}\varepsilon \quad (4)$$

$$S_{\rm el}(V,T) = -k_{\rm B}\int n(\varepsilon,V)\{f(\varepsilon)\ln f(\varepsilon) + [1-f(\varepsilon)]\ln[1-f(\varepsilon)]\}{\rm d}\varepsilon \quad (5)$$

where $k_{\rm B}$ is the Boltzmanns constant, T the temperature, $n(\varepsilon,V)$ the electronic DOS, $f(\varepsilon)$ the Fermi function, ω_j the vibrational frequency, ε_F the total density of states at Fermi energy level, n the number of atoms, and N the number of cells in the macroscopic solid [19]. Thermal properties such as heat capacity C_V, C_P, isothermal bulk modulus B_T, adiabatic bulk modulus B_S, thermal expansion coefficient α, Grüneisen ratio γ and entropy S can be deriven from Eq.(1)

$$C_V = \sum k_{\rm B}\left(\frac{\omega_j}{k_{\rm B}T}\right)^2\frac{{\rm e}^{-\omega_j/k_{\rm B}T}}{({\rm e}^{-\omega_j/k_{\rm B}T}-1)^2} \quad (6)$$

$$C_P = C_V(1+\gamma\alpha T) \quad (7)$$

$$B_T = V\left(\frac{\partial^2 F}{\partial V^2}\right)_T \quad (8)$$

$$B_S = B_T(1+\gamma\alpha T) \quad (9)$$

$$\alpha = \frac{\gamma C_V}{VB_T} \quad (10)$$

$$\gamma = -\frac{V}{TC_V}\frac{\partial(-TS)}{\partial V} \quad (11)$$

$$S = \sum\left[-k_{\rm B}\ln(1-e^{-\omega_j/k_{\rm B}T}) + \frac{\omega_j}{T}\frac{1}{e^{\omega_j/k_{\rm B}T}-1}\right] \quad (12)$$

The advantages of the FEQHA scheme are: (i) wide ranges of temperature and pressure conditions are considered, (ii) only a few calculation parameters are included in this approach. Up to now, the magnetic energies of solids are not considered in the QHA and FEQHA methods. Therefore, these methods are not suitable for transition metals and the corresponding alloys. On the other hand, the high-temperature results obtained by QHA near the melting point $T_{\rm m}$ ($T-T_{\rm m}$<100 K) have not been verified by experiments. The disadvantage of QHA, however, is that most of the parameters are nonlinear and starting from a good set of values is usually a requirement for achieving the convergence of the total energies. Appling the FEQHA model, the real situations inside solids can be simulated well since the mobile electrons are included.

III. RESULTS AND DISCUSSION

A. Crystal structures and elastic properties

The schematic crystal structures and different atomic coordinations of Al, NiAl and Ni_3Al are plotted in Fig.1. The pressure effect on the elastic constants is essential, especially for understanding the chemical interaction and mechanical stability, and for for developing interatomic potentials. Therefore, the dependences of the elastic constants on pressure for Al, NiAl and Ni_3Al are calculated and listed in Tables I and II. According to the

DOI:10.1063/1674-0068/27/04/399-406

TABLE I Lattice constant a, elastic constants C_{ij}, bulk modulus B, shear modulus G, Young's modulus E, Poisson's ratio σ and Zeners elastic anisotropy A of Al.

P/GPa	a/nm	C_{11}/GPa	C_{12}/GPa	C_{44}/GPa	B/GPa	G/GPa	B/G	A	E/GPa	σ	B^{FEQHA}/GPa
0	0.4049	95.8	70.6	17.2	79.1	15.2	5.203	1.365	42.8	0.409	78.3
40	0.3685	292.7	193.9	123.0	226.8	85.3	2.658	2.489	227.3	0.332	229.4
80	0.3516	457.8	297.8	193.1	351.1	135.6	2.589	2.413	360.4	0.328	355.4
120	0.3402	588.5	402.9	213.8	464.8	152.9	3.039	2.303	413.3	0.351	473.2
160	0.3315	739.7	490.6	257.5	573.7	192.4	2.981	2.067	519.1	0.349	579.8
200	0.3246	902.9	570.6	318.4	681.4	245.3	2.777	1.916	657.1	0.339	698.1
Expt. [31]	0.4049	114.3	61.9	31.6							
Expt. [34]	0.4050										
Expt. [32]		106.8	60.7	28.2	79.4						
Calc. [35]	0.4051										
Calc. [20]	0.3969	115.0	52.0	32.0							
Calc. [19]	0.4067										
Calc. [33]	0.4038	107.0	60.0	28.0							
Calc. [14]		106.9	60.7	28.3	72.9						

P of experimental and calculated parameters in all references is 0 GPa.

TABLE II Lattice constant a, elastic constants C_{ij}, bulk modulus B, shear modulus G, Young's modulus E, Poisson's ratio σ and Zeners elastic anisotropy A of NiAl and Ni_3Al.

	P/GPa	a/nm	C_{11}/GPa	C_{12}/GPa	C_{44}/GPa	B/GPa	G/GPa	B/G	A	E/GPa	σ
NiAl	0	0.2899	190.3	141.4	111.6	157.7	61.4	2.568	4.563	163.0	0.327
	10	0.2845	237.2	179.8	132.1	198.9	72.4	2.746	4.604	193.8	0.337
	20	0.2802	283.7	216.2	151.8	238.7	83.9	2.845	4.502	225.3	0.342
	30	0.2766	329.7	251.2	172.3	277.3	96.1	2.884	4.385	258.5	0.344
	0 [6]		198±5	137±3	116±3	157.3	68.2	2.305	3.740	178.8	0.311
Ni_3Al	0	0.3576	278.6	134.1	65.1	182.3	67.9	2.684	0.901	181.2	0.334
	10	0.3518	340.2	171.2	76.4	227.6	79.5	2.859	0.905	213.8	0.343
	20	0.3472	397.7	207.0	86.0	270.6	89.6	3.018	0.902	242.2	0.351
	30	0.3432	452.8	241.8	94.9	312.1	99.0	3.152	0.899	268.6	0.356
	0 [22]		225.3	157.6	121.1	180.2	72.9	2.472	3.577	192.7	0.322
	0 [37]		221.0	146.0	124.0	171.0	76.9	2.224	3.306	200.6	0.304

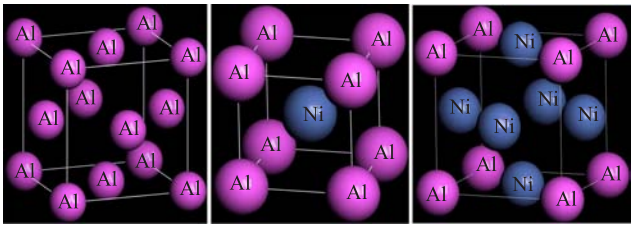

FIG. 1 Crystal structures and atomic arrangements of (a) Al, (b) NiAl, and (c) Ni_3Al.

Voigt-Reuss-Hill (VRH) approach [30], the bulk modulus B, shear modulus G, Young's modulus E, Poisson's ratio σ, and Zeners elastic anisotropy factor A for the cubic crystal can be determined by the following equations [6, 22]

$$B = \frac{1}{3}(C_{11} + 2C_{12}) \tag{13}$$

$$G = \frac{1}{2}\left[\frac{1}{5}(C_{11} - C_{12} + 3C_{44}) + \frac{5(C_{11} - C_{12})C_{44}}{3(C_{11} - C_{12}) + 4C_{44}}\right] \tag{14}$$

$$E = \frac{9GB}{3B + G} \tag{15}$$

$$\sigma = \frac{3B - E}{6B} \tag{16}$$

$$A = \frac{2C_{44}}{C_{11} - C_{12}} \tag{17}$$

DOI:10.1063/1674-0068/27/04/399-406

As shown in Table I, the lattice constant a, elastic constants C_{ij}, elastic modulus B, G and E of Al are consistent with the experimental data as well as with the theoretical results. The elastic constants and elastic moduli increase with applied pressure while a shows the opposite trend. The slopes of these quantities are different. C_{11} is more sensitive to pressure than C_{12} and C_{44}. At 0 GPa, the discrepancy between the calculated C_{ij} and the experimental data [31, 32] is mainly due to: (i) GGA typically underestimates the elastic constants; (ii) the experimental data are obtained at room temperature while first-principles results are restricted to 0 K; (iii) The measurements of C_{ij} from polycrystalline samples include defects and porosities. In our scheme, the calculations are related to ideal crystals. The Born and Huangs stability criteria [36] ($C_{11}+2C_{12}>0$, $C_{44}>0$, $C_{11}-C_{12}>0$ and $C_{11}>B>C_{12}$) are satisfied by the elastic constants listed in Table I. Therefore, Al can retain its cubic structure in the pressure range of 0−200 GPa. σ decreases first, and then increases or decreases unorderedly when the pressure exceeds 80 GPa. It is worth noting that the PW-PP bulk moduli agree well with the FEQHA bulk moduli, which have partially proven the reliability of our calculation.

As it can be seen in Table II, C_{11} and C_{12} of NiAl and Ni_3Al increase monotonically and rapidly with applied pressure while C_{44} increases slowly with pressure increasing. All B, G and E increase with the increasing pressure, but the slopes are different. σ is larger than 0.327 (0.334) for NiAl (Ni_3Al) and gradually increases with applied pressure. C_{ij} satisfies the Born and Huangs criteria [36], which suggests that the cubic Ni_xAl (x=1, 3) are stable below 30 GPa. The elastic anisotropy can be conveniently expressed by a dimensionless parameter A, which is called Zeners elastic shear anisotropy factor. A=1 reflects the isotropic character of a crystal, but a majority of solids show elastic anisotropy ($A\neq1$). For NiAl, A increases with the increasing pressure up to 10 GPa whereas it decreases linearly in the pressure range of 10−30 GPa. Ni_3Al is little anisotropic and somewhat insensitive to pressure. Besides, the anisotropy of Al (see Table I) increases rapidly with pressure when P<40 GPa and gradually becomes less anisotropic upon further compression.

Pugh introduced the B/G ratio characterized as an indication of brittle versus ductile [38]. If B/G>1.75, the material exhibits a ductile manner, otherwise, it behaves in a brittle character. Besides, the smaller the B/G ratio is, the stronger the material hardness will be. The B/G ratio indicates that NiAl and Ni_3Al are ductile alloys. The ductility increases with the increasing pressure. NiAl is harder than Ni_3Al at a fixed pressure. As can be seen in Table I, Al is a brittle material at 0 GPa, but it behaves in ductile manner in the pressure range of 40−200 GPa. Our calculated zero-pressure lattice constant of NiAl agrees well with the theoretical values (0.2918 Å [7], 0.2895 Å [39]) and the experimental data (0.2880 Å [40]). The lattice constant of Ni_3Al is also in excellent agreement with the theoretical results (0.3568 Å [10], 0.3574 Å [22]) and the experimental data (0.3572 Å [41]). All the values listed in Table II are in agreement with the results reported in Refs.[6, 22, 37] except C_{44} and A of Ni_3Al. Unfortunately, the exact reason for this discrepancy is still unclear.

B. Thermal properties

Since Ni_xAl (x=0, 1 and 3) are potential materials for satellite components and deoxidizers, it is necessary to investigate the thermal properties of Al, NiAl and Ni_3Al under extreme conditions. For the NiAl and Ni_3Al alloys, the Debye-Grneisen model is used in the FEQHA scheme.

Figure 2(a) displays the temperature dependence of α for Al via different methods. After a sharp increase, up to 300 K, α reaches a linear region in the temperature range of 300−900 K. It can be clearly seen that the FEQHA results are closer to the experimental data [42] in the temperature range of 0−400 K compared with the QHD results. The results of these two approaches agree well with the experimental data [42] at temperatures higher than 400 K. In Ref.[19], the computed α of Al, Ni, NiAl and Ni_3Al are often larger than the experimental data at high temperature. Generally speaking, our FEQHA results are more reliable than the QHD results since the electron contributions are taken into account in the FEQHA approach. As shown in Fig.2(b), the behavior of α is quite different. The 0 GPa-curve has a parabolic behavior while the 200 GPa-curve shows almost linear dependence on temperature. α decreases rapidly as the pressure increases. The temperature effect becomes less important.

Figure 2 (c) and (d) illustrate the pressure and temperature effects on the thermal expansion coefficient α of NiAl and Ni_3Al, respectively. Both pressure and temperature are important for α. At a given temperature, α increases with the decreasing pressure. At a fixed pressure, α increases sharply with the increasing temperature below 400 K. Then, the rate decreases in the temperature range of 400−1300 K. The calculated thermal expansion coefficients of NiAl and Ni_3Al are basically closer to the reported experimental data [42] compared with the theoretical results given in Ref.[19]. At high temperatures, Al has the greatest α while Ni_3Al has the lowest α. The thermal expansion decreases with the subscript x of the Ni_xAl crystal.

The isobaric heat capacity C_P and isochoric heat capacity C_V of Al, NiAl and Ni_3Al on the temperature and pressure dependences are drawn in Fig.3 and Fig.4, repectively. As shown in Fig.3(a), C_P increases quickly at low temperature and tends to zero when the temperature vanishes. Then, C_P gradually reaches a linear region (T>400 K) and the propensity of increment becomes gentler. One can also notice that the FEQHA results are rather in good agreement with the exper-

DOI:10.1063/1674-0068/27/04/399-406

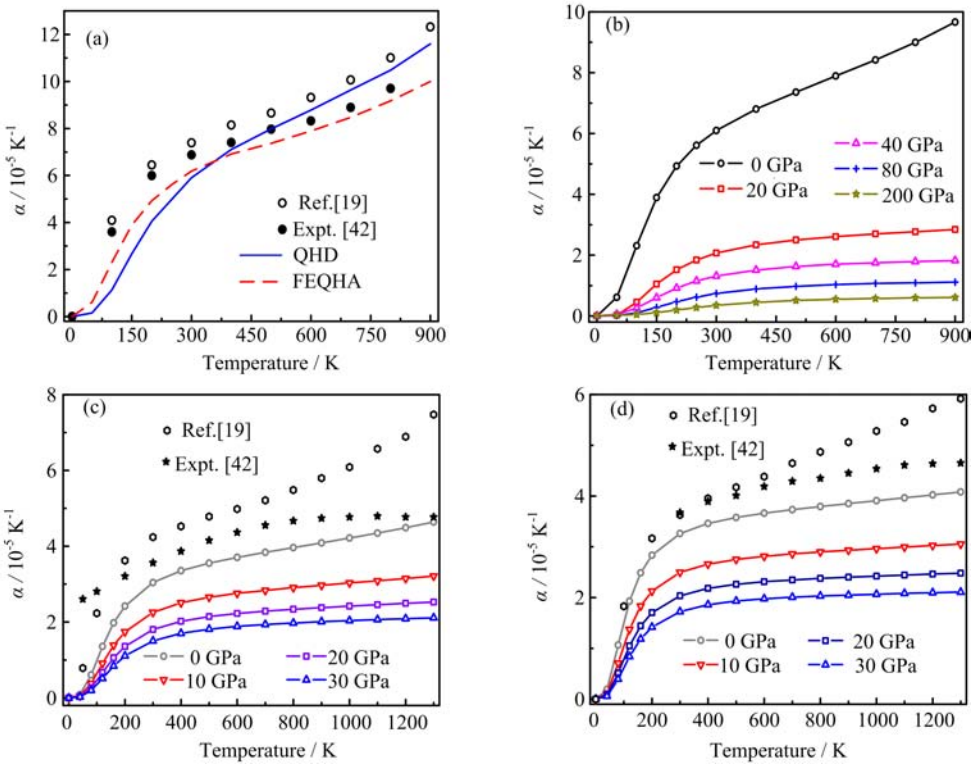

FIG. 2 (a) Temperature dependence of α for Al. Variations of α with temperature and pressure for (b) Al, (c) NiAl, and (d) Ni_3Al.

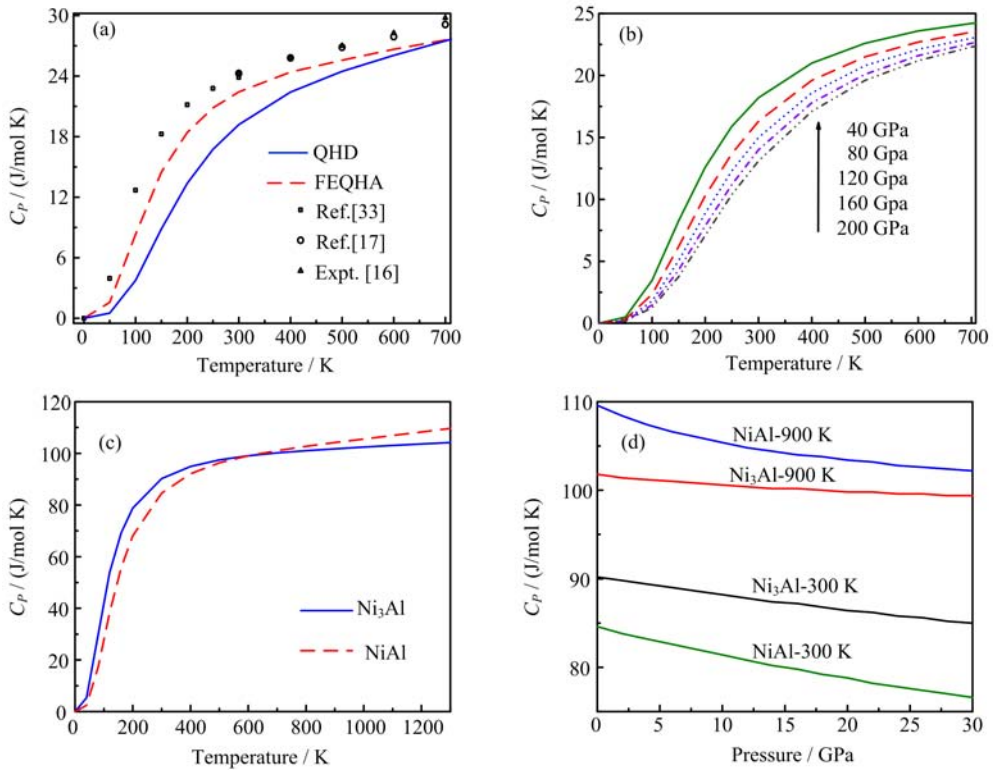

FIG. 3 (a) Temperature dependence of C_P for Al at 0 GPa. (b) Variations of C_P for Al with temperature at 40, 80, 120, 160, 200 GPa. (c) Temperature dependences of C_P for NiAl and Ni_3Al at 0 GPa. (d) Pressure dependences of C_P for NiAl and Ni_3Al.

DOI:10.1063/1674-0068/27/04/399-406

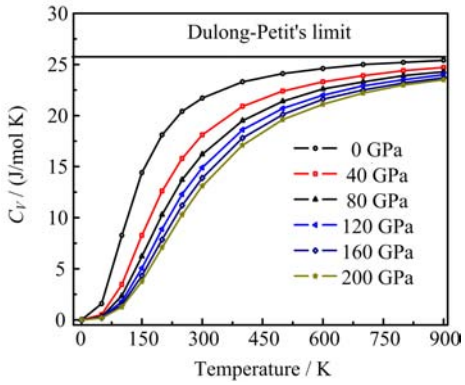

FIG. 4 Variations of C_V for Al with temperature and pressure.

imental data [16] and the theoretical results [17, 33] compared with the QHD results. It is found in Fig.3(b) that C_P is dependent on both temperature and pressure. C_P increases with the temperature at a given pressure, and decreases with the pressure when the temperature is fixed. The temperature effect on C_P is much more significant than that of pressure. As shown in Fig.4, C_V follows the Debye T^3 law at low temperatures. C_V and C_P show roughly similar behaviors in the entire ranges of pressure 0−200 GPa and the temperature 0−700 K. Unlike the isobaric heat capacity curves, the C_V curves obey to the Dulong and Petits classical law (24.94 J/(mol K): $C_V \sim 3R$ for monoatomic materials) at high temperatures while C_P follows a linear increase with the temperature increasing.

In Fig.3(c), C_P shows a sharp increase up to 300 K, and then C_P increases almost linearly with the temperature increasing. The C_P values of Ni_3Al are larger than those of NiAl before the cross point (at 600 K). It is seen from Fig.3(d) that C_P decreases at the given temperature when the pressure increases. The influences of the temperature on C_P are much more significant than that of the pressure on it. The calculated C_P for Ni_3Al are 90.2, 97.8, 100.9 and 102.7 J/(mol K) at temperatures of 300, 500, 700 and 900 K, respectively. These values are in agreement with the experimental data of 97.9 (300 K), 103.7 (500 K), 109.3 (700 K) and 115.6 J/(mol K) (900 K) [23]. The calculated C_P are consistent with Shang *et al.*'s results [23], which reflects that our results are reliable.

Figure 5(a) shows the temperature dependences of the isothermal bulk modulus B_T ($B_{T(P=0)}$=B) and adiabatic bulk modulus B_S for Al. One can see that B_T and B_S are nearly constant from 0 K to 100 K, which indicates that the temperature effect on bulk modulus is trivial. This is due mainly to the fact that the atomic vibrations in the unit cell are not significant in the temperature range of 0−100 K. As calculated obviously from Eq.(9), B_T and B_S coincide at zero temperature and diverge more and more when the temperature increases. B_S decreases moderately and smoothly with

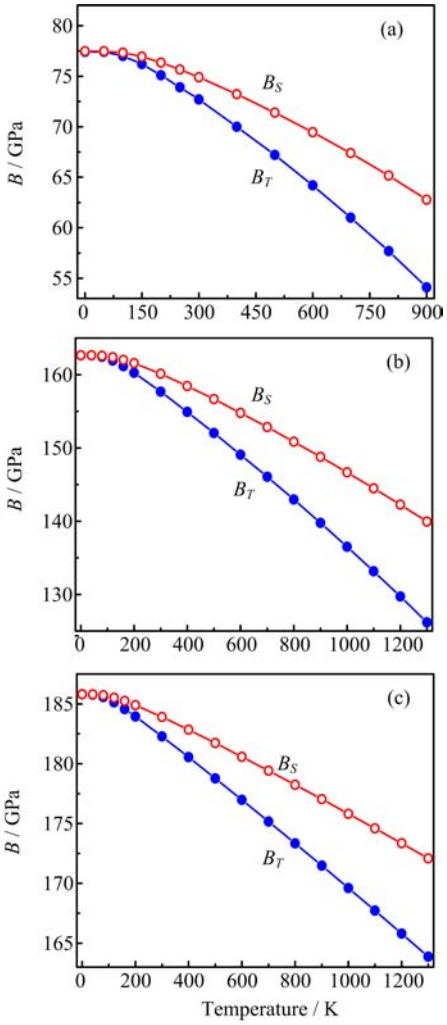

FIG. 5 The temperature dependences of adiabatic bulk modulus B_S and isothermal bulk modulus B_T for (a) Al, (b) NiAl, and (c) Ni_3Al.

the temperature increasing. The negative slopes of the curves demonstrate that Al becomes more and more compressible when T is applied and the compressibility increases with the increasing temperature. It is the rapid volume variation that makes B_T rapidly decrease. The calculated B_S are 74.9, 71.4, 67.4, and 62.7 GPa at temperatures of 300, 500, 700, and 900 K, respectively. These results are in good agreement with the experimental B_S values of 76.1 (at 300 K), 72.5 (at 500 K), 68.3 (at 700 K) and 63.9 GPa (at 900 K) [43].

It can be clearly seen from Fig.5 (b) and (c) that the temperature dependences of B_S and B_T for NiAl, and Ni_3Al are quite similar to the curves drawn in Fig.5(a). In the temperature range of 0−1300 K, B_S (B_T) decreases by 19.01% (30.10%), 13.96% (22.38%), and 7.37% (11.84%) for Al, NiAl, and Ni_3Al, respectively. Therefore, the temperature effect on the compressibility of NiAl is weaker than that of Al, but stronger than that of Ni_3Al. Since Eq.(9), errors in the higher-order

DOI:10.1063/1674-0068/27/04/399-406

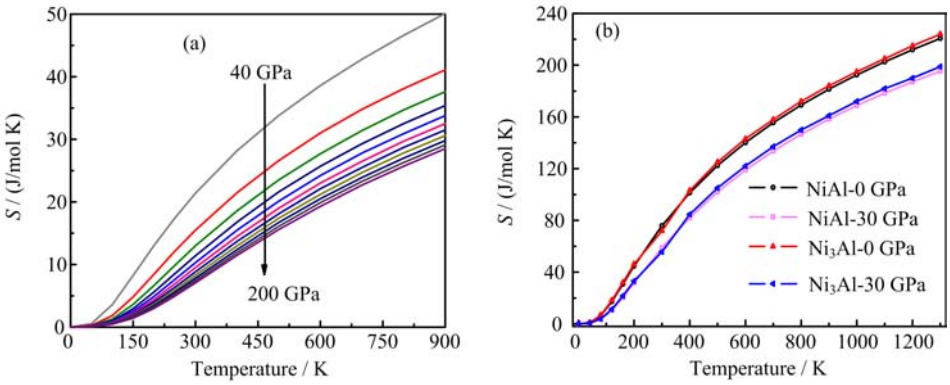

FIG. 6 The temperature dependences of entropy S for (a) Al at 0, 20, 40, 60, 80, 100, 120, 140, 160, 180, and 200 GPa shown as the arrow indicates, (b) NiAl and Ni_3Al.

thermal parameters (the thermal expansion coefficient α and the Grüneisen parameter γ) will lead to larger errors in the isothermal bulk modulus B_T. As shown in Fig.5(c), the calculated B_T (Ni_3Al) are 183.9, 178.4 and 171.2 GPa at temperatures of 300, 700 and 1300 K, respectively. These results agree well with the theoretical values of 173.9 (300 K), 164.5 (700 K) and 151.8 (1300 K) [23]. More importantly, the FEQHA bulk moduli of the three alloys are in agreement with the PW-PP bulk moduli listed in Tables I and II.

In Fig.6(a), the entropy S of Al is very small below 100 K. Between 100 and 900 K, the entropy, as expected, increases quickly with the increasing temperature. When the pressure increases from 0 to 200 GPa, the entropy S decreases at constant temperature. The effect of increasing the temperature is similar to decreasing the pressure. The entropy S drawn in Fig.6(b) shows the same performance as the entropy illustrated in Fig.6(a). S is variable by power exponent with the temperature increasing. Ni_3Al has greater entropies compared with NiAl. The temperature effect on S is much more significant than the pressure effect on S. Our calculated entropies for Ni_3Al are 0.88 at 40 K, 71.94 at 300 K and 184.79 J/(mol K) at 900 K, agreeing with the theoretical results of 0.99 at 40 K, 97.37 at 300 K and 215.17 J/(mol K) at 900 K [23].

IV. CONCLUSION

The structural, elastic and thermodynamic properties of the typical metal Al and its alloys (NiAl, Ni_3Al) have been investigated through the accurate plane-wave pseudo-potential method combined with the full-electronic quasi-harmonic approximation (where the highly mobile electrons are included). The agreement between our calculated lattice constants/elastic constants and the other results is good. All the elastic constants meet the mechanical stability criteria. B/G ratios are well above 2.56 suggesting NiAl and Ni_3Al as ductile. Ni_3Al is little anisotropic and somewhat insensitive to pressure. Both NiAl and Al have strong elastic anisotropies. The bulk modulus, heat capacity, thermal expansion coefficient and entropy of Al, NiAl and Ni_3Al are predicted at simultaneously high temperatures and high pressures. The results show that Al has the greatest thermal expansion cofficient while Ni_3Al has the lowest one. Ni_3Al has greater entropies compared with NiAl. Some interesting features in these quantities can be observed at high temperatures.

The agreement between our computed thermal properties and the available experimental data indicates that the FEQHA approach can predict blindly the behaviors of Ni-Al alloys in regions beyond the experimental limits. Nevertheless, our results are all predictions and need to be verified by the future experiments.

V. ACKNOWLEDGEMENTS

This work was supported by the National Natural Science Foundation of China (No.U1204501, No.11304141, No.11105115). We thank Prof. Alberto Qtero-de-la-Roza and his colleague for the FEQHA model (Gibbs2 code). We also acknowledge Prof. M. A. Blanco and his co-workers for their QHD model (Gibbs code).

[1] T. G. White, S. Richardson, B. J. B. Crowley, L. K. Pattison, J. W. O. Harris, and G. Gregori, Phys. Rev. Lett. **111**, 175002 (2013).
[2] J. C. Boettger and S. B. Trickey, Phys. Rev. B **53**, 3007 (1996).
[3] R. G. Greene, H. Luo, and A. L. Ruoff, Phys. Rev. Lett. **73**, 2075 (1994).
[4] J. Q. He, Y. Wang, M. F. Yan, Y. Yang, and L. Wang, Comput. Mater. Sci. **50**, 545 (2010).
[5] S. He, P. Peng, L. Peng, Y. Chen, H. Wei, and Z. Q. Hu, J. Alloys Compd. **597**, 243 (2014).
[6] G. Frommeyer, R. Rablbauer, and H. J. Schäfer, Intermetallics **18**, 299 (2010).

DOI:10.1063/1674-0068/27/04/399-406

[7] H. Z. Fu, Z. F. Hou, J. Fu, and Y. M. Ma, Intermetallics **42**, 156 (2013).
[8] Z. F. Zhang, B. Gleeson, K. Y. Jung, L. Li, and J. C. Yang, Acta Mater. **60**, 5273 (2012).
[9] J. Zhang, Z. Chen, X. J. Du, C. Chen, and T. Yang, Superlattices Microstruct. **52**, 834 (2012).
[10] A. Hussain, S. Aryal, P. Ruils, M. A. Choudhry, J. Chen, and W. Y. Ching, J. Alloys Compd. **509**, 5230 (2011).
[11] M. A. Blanco, E. Francisco, and V. Luaña, Comput. Phys. Commun. **158**, 57 (2004).
[12] D. W. He, Y. S. Zhao, L. L. Daemen, J. Qian, K. Lokshin, T. D. Shen, J. Zhang, and A. C. Lawson, J. Appl. Phys. **95**, 4645 (2004).
[13] A. R. Shirani Bidabadi, M. H. Enayati, E. Dastanpoor, R. A. Varin, and M. Biglari, J. Alloys Compd. **581**, 91 (2013).
[14] P. S. Ho and A. L. Ruoff, J. Appl. Phys. **40**, 3151 (1969).
[15] N. W. Ashcroft and N. D. Mermin, *Solid State Physics*, New York: Rinehar and Winston, (1976).
[16] R. C. Shukla and C. A. Plint, Int. J. Thermophys. **1**, 299 (1980).
[17] S. Raju, K. Sivasubramanian, and E. Mohandas, Solid State Commun. **122**, 671 (2002).
[18] Y. P. Varshni and R. C. Shukla, J. Chem. Phys. **43**, 3966 (1965).
[19] Y. Wang, Z. K. Liu, and L. Q. Chen, Acta Mater. **52**, 2665 (2004).
[20] A. Debernardi, M. Alouani, and H. Dreyssé, Phys. Rev. B **63**, 064305 (2001).
[21] S. K. Xiang, L. C. Cai, and F. Q. Jing, Phys. Rev. B **70**, 174102 (2004).
[22] H. Hou, Z. Q. Wen, Y. H. Zhao, L. Fu, N. Wang, and P. Han, Intermetallics **44**, 110 (2014).
[23] S. L. Shang, Y. Wang, D. E. Kim, and Z. K. Liu, Comput. Mater. Sci. **47**, 1040 (2010).
[24] W. Kohn and L. J. Sham, Phys. Rev. **140**, A1133 (1965).
[25] J. P. Perdew, K. Burke, and M. Ernzerhof, Phys. Rev. Lett. **77**, 3865 (1996).
[26] H. J. Monkhorst and J. D. Pack, Phys. Rev. B **13**, 5188 (1976).
[27] G. J. Ackland, M. C. Warren, and S. J. Clark, J. Phys.: Condens. Matter **9**, 7861 (1997).
[28] A. Otero-de-la-Roza and V. Luaña, Comput. Phys. Commun. **182**, 1708 (2011).
[29] A. Otero-de-la-Roza and V. Luaña, Comput. Phys. Commun. **182**, 2232 (2011).
[30] R. Hill, Proc. Phys. Soc. A **65**, 349 (1952).
[31] G. N. Kamm and G. A. Alers, J. Appl. Phys. **35**, 327 (1964).
[32] K. Hachiya and Y. Ito, J. Alloys Compd. **337**, 53 (2002).
[33] D. R. Lide, *Handbook of Chemistry and Physics*, New York: CRC Press, (1998).
[34] R. Gaudoin, W. M. C. Foulkes, and G. Rajagopal, J. Phys.: Condens. Matter **14**, 8787 (2002).
[35] B. K. Panda, C. D. Beling, and S. Fung, Phys. Rev. B **50**, 5695 (1994).
[36] M. Born and K. Huang, *Dynamical Theory of Crystal Lattices*, Oxford: Clarendon, (1954).
[37] H. Yasuda, T. Takasugi, and M. Koiwa, Acta Metall. Mater. **40**, 381 (1992).
[38] S. F. Pugh, Philos. Mag. **45**, 823 (1954).
[39] N. I. Papanicolaou, H. Chamati, G. A. Evangelakis, and D. A. Papaconstantopoulos, Comput. Mater. Sci. **27**, 191 (2003).
[40] Y. I. Dutchak and V. G. Chekh, Russ. J. Phys. Chem. **55**, 1326 (1981).
[41] P. M. Rao, S. Suryanarayana, K. S. Murthy, and S. N. Naidu, J. Phys.: Condens. Matter **1**, 5357 (1989).
[42] Y. S. Touloukian, R. K. Kirby, R. E. Taylor, and P. D. Desai, *Thermal Expansion: Metallic Elements and Alloys*, New York: Plenum Press, (1975).
[43] D. Gerlich and E. S. Fisher, J. Phys. Chem. Solids **30**, 1197 (1969).

DOI:10.1063/1674-0068/27/04/399-406